

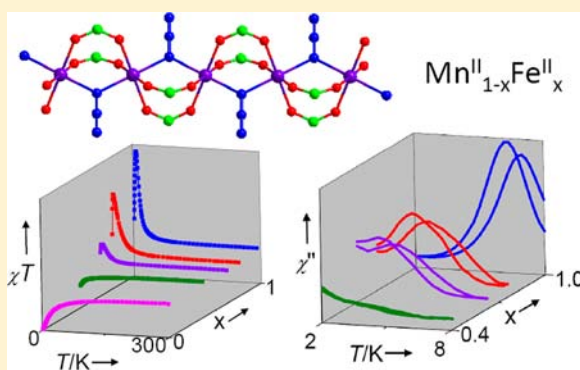
Manganese(II), Iron(II), and Mixed-Metal Metal–Organic Frameworks Based on Chains with Mixed Carboxylate and Azide Bridges: Magnetic Coupling and Slow Relaxation

Yan-Qin Wang, Qi Yue, Yan Qi, Kun Wang, Qian Sun, and En-Qing Gao*

†Shanghai Key Laboratory of Green Chemistry and Chemical Processes, Department of Chemistry, East China Normal University, Shanghai 200062, People's Republic of China

Supporting Information

ABSTRACT: Mn(II) and Fe(II) compounds derived from azide and the zwitterionic 1-carboxylatomethylpyridinium-4-carboxylate ligand are isomorphous three-dimensional metal–organic frameworks (MOFs) with the *sra* net, in which the metal ions are connected into anionic chains by mixed (μ -1,1-azide)bis(μ -carboxylate) triple bridges and the chains are cross-linked by the cationic backbones of the zwitterionic ligands. The Mn(II) MOFs display typical one-dimensional antiferromagnetic behavior. In contrast, with one more d electron per metal center, the Fe(II) counterpart shows intrachain ferromagnetic interactions and slow relaxation of magnetization attributable to the single-chain components. The activation energies for magnetization reversal in the infinite- and finite-chain regimes are $\Delta_{r1} = 154$ K and $\Delta_{r2} = 124$ K, respectively. Taking advantage of the isomorphism between the Mn(II) and Fe(II) MOFs, we have prepared a series of mixed-metal $\text{Mn}^{II}_{1-x}\text{Fe}^{II}_x$ MOFs with $x = 0.41, 0.63,$ and 0.76 , which intrinsically feature random isotropic/anisotropic sites and competing antiferromagnetic–ferromagnetic interactions. The materials show a gradual antiferromagnetic-to-ferromagnetic evolution in overall behaviors as the Fe(II) content increases, and the Fe-rich materials show complex relaxation processes that may arise for mixed SCM and spin-glass mechanisms. A general trend is that the activation energy and the blocking temperature increase with the Fe(II) content, emphasizing the importance of anisotropy for slow relaxation of magnetization.



INTRODUCTION

Molecular magnetic systems in which paramagnetic metal ions are held in close proximity by short bridges have been intensely studied for decades to uncover new magnetic phenomena and the underlying physics and to obtain new magnetic materials with potential applications. In the past decade, considerable attention has been paid to the so-called single-chain magnets (SCMs), which are one-dimensional (1D) systems exhibiting freezable magnetization associated with slow relaxation.^{1,2} The slow magnetic dynamics of an SCM arises from two essential elements: (i) a 1D noncanceling (ferromagnetic (FO), ferrimagnetic (FI), or canted antiferromagnetic (AF)) arrangement of spin carriers and (ii) a large uniaxial anisotropy. The design of SCMs requires elaborate choices of the metal ions and the bridging ligands, and several synthetic strategies to specific SCM systems have been developed. Most of the reported SCMs are heterospin systems, perhaps due to the ease in achieving FO and FI arrangements with dissimilar spins, such as M–radical (M = Co^{II}, Mn^{III}, Dy^{III}, Ho^{III}),^{1b,2,3} Mn^{III}–Ni^{II} with oximate bridges,^{1c,2,4} various bi- and even trimetallic combination with cyano bridges,^{2,5,6} Co^{II}–M (M = Cu^{II}, Cr^{III} or Fe^{III}) with oxamate or oxalato bridges,^{2,7} and Fe^{II}–Fe^{III} with *N*-carbonylamide or carboxylate bridges,⁸ where the required magnetic anisotropy comes from at least one of the spin

carriers. A limited but increasing number of homospin SCMs have emerged in recent years, mainly involving Co^{II} or Mn^{III} as anisotropic spin carriers with azide,⁹ carboxylate,¹⁰ or phosphonate¹¹ as bridging groups. Homospin SCMs with other metal ions (such as Fe^{II} and Dy^{III}) or other bridges (such as tetrazolate and even π – π interactions) are also known but still rare.^{12–14}

Although the family of SCMs has become quite large, the rational design of new SCMs (especially the homospin ones) and the tuning of SCM properties are still great challenges. In addition to the two basic requirements relevant to the anisotropy and intrachain interactions, it is also required that interchain interactions should be much weaker than intrachain interactions to ensure the SCM dynamics. For this purpose, bulky organic ligands have been used to avoid close contacts between chains. An alternative strategy is to construct 2D or 3D metal–organic frameworks (MOFs) in which magnetic chains are structurally linked to but magnetically isolated from each other by interchain ligands.^{8e,10,12b,13a,14a,b} This strategy has great potential, considering the rapid development of MOFs in recent years.¹⁵

Received: October 4, 2012

Published: April 3, 2013

We have recently demonstrated that the use of zwitterionic pyridinium-carboxylate ligands as carboxylate sources is an easy and efficient synthetic approach toward magnetic systems with mixed pseudohalide and carboxylate bridges.^{16–18} The zwitterionic nature of the carboxylate ligands helps to balance the competition between the two anionic bridges in binding metal cations. The approach has led to various mixed-bridge motifs, including polynuclear clusters, infinite chains and layers, and even 3D frameworks. The most frequently encountered are chain motifs with $(\mu-1,1-N_3)(\mu-COO)_2$ or $(\mu-1,1-N_3)_2(\mu-COO)$ triple bridges, and some Co(II) compounds, including 1D coordination polymers and 2D chain-based MOFs derived from zwitterionic monocarboxylates and dicarboxylates, respectively, have been demonstrated to show SCM dynamics,¹⁸ benefiting from the FO coupling through the mixed bridges and the large anisotropy of Co(II). Further along this line, here we report on the isomorphous Mn(II) and Fe(II) 3D MOFs in which chains with $(\mu-1,1-N_3)(\mu-COO)_2$ bridges are linked by zwitterionic 1-carboxylatomethylpyridinium-4-carboxylate (cmcp) ligands. The Mn(II) MOF exhibits typical 1D antiferromagnetism, while the Fe(II) counterpart exhibits 1D ferromagnetism and slow magnetic relaxation, representing the first Fe(II) SCM with mixed carboxylate and azide bridges.

On the basis of the isomorphism of the Mn(II) and Fe(II) MOFs, we also report on a series of $Mn^{II}_{1-x}Fe^{II}_x$ MOFs with variable metal ratios. The mixed-metal systems are solid solutions with random metal sites, in contrast with the known heterometallic SCMs that have fixed metal ratios and have different coordination sites for different metal ions. Magnetic mixed-metal solid solutions, including mainly inorganic magnets (alloys, metal oxides, and salts) and occasionally molecular magnets, have been studied.^{19–22} The variable composition in conjunction with the site randomness can lead to tuned and sometimes unusual magnetic properties. For example, systems with competing AF and FO interactions can have spin-glass states,¹⁹ and those with competing single-ion anisotropies can exhibit tetra-critical-point phase diagrams.²⁰ The present $Mn^{II}_{1-x}Fe^{II}_x$ MOFs represent a nice example of isomorphous quasi-1D magnetic systems featuring random isotropic/anisotropic sites and competing AF/FO interactions, allowing us to observe a gradual evolution from 1D antiferromagnetism to 1D ferromagnetism with complex relaxation behaviors.

EXPERIMENTAL SECTION

Synthesis. Reagents were obtained from commercial sources and used as received. 1-Carboxymethylpyridinium-4-carboxylate (Hcmcp) was prepared according to the literature.²³

Caution! Although we did not encounter this in our experiments, azido compounds of metal ions are potentially explosive. Only a small amount of the materials should be prepared, and they should be handled with care.

[Mn(cmcp)(N₃)]·H₂O (1). A mixture of Mn(OAc)₂·4H₂O (0.049 g, 0.20 mmol), NaN₃ (0.026 g, 0.40 mmol), and Hcmcp (0.018 g, 0.10 mmol) in water/ethanol (3/4 mL) was stirred for 10 min at room temperature. Slow evaporation of the solution at room temperature yielded yellow crystals of **1** after 2 days. Yield: 51% based on Hcmcp. Anal. Calcd for C₈H₈MnN₄O₅: C, 32.56; H, 2.73; N, 18.98. Found: C, 32.69; H, 3.01; N, 19.42%. Main IR bands (KBr, cm⁻¹): $\nu(N_3)$ 2070 vs, $\nu(COO)$ 1630 s and 1390 s.

[Fe(cmcp)(N₃)]·H₂O (2). A methanol solution (4 mL) of Fe(ClO₄)₂·9H₂O (0.13 g, 0.32 mmol) (a small amount of ascorbic acid had been added to avoid the oxidation of Fe(II)) and an aqueous solution (2 mL) of Hcmcp (0.11 g, 0.60 mmol) were mixed with stirring. The colorless solution was refluxed under a N₂ atmosphere

while sodium azide (0.13 g, 2.0 mmol) was added, yielding black polycrystals immediately. After the solution was refluxed for 3 h, the polycrystals were collected by filtration, washed with water and methanol, and dried in air. Yield: 60% based on Fe. Anal. Calcd for C₈H₈FeN₄O₅: C, 32.46; H, 2.72; N, 18.93. Found: C, 32.65; H, 2.97; N, 18.93. Main IR bands (cm⁻¹, KBr): $\nu(N_3)$ 2070 vs, $\nu(COO)$ 1618 s and 1380 s. Efforts to grow crystals of **2** suitable for single-crystal X-ray analyses were unsuccessful.

[Mn^{II}_{1-x}Fe^{II}_x(cmcp)(N₃)]·H₂O. These heterometallic compounds were synthesized by procedures similar to those for **2**, using methanol solutions containing Fe(ClO₄)₂·9H₂O and Mn(OAc)₂·4H₂O in different molar ratios (Mn:Fe = 1:1, 2:3, 1:4). Yields: 30–60%. According to analyses using inductively coupled plasma (ICP) spectrometry, the Mn:Fe molar ratios in the products are 0.59:0.41, 0.37:0.63, and 0.24:0.76. Typical IR (cm⁻¹, KBr): $\nu(N_3)$ 2070 s, $\nu(COO)$ 1625 s and 1383 s. The C/H/N elemental analysis results of the three compounds are identical within experimental error.

Physical Measurements. Elemental analyses (C, H, and N) were performed on a Perkin-Elmer 2400 CHN elemental analyzer. FT-IR spectra were recorded in the range 500–4000 cm⁻¹ on a Nicolet NEXUS 670 spectrophotometer using KBr pellets. The X-ray diffraction (XRD) patterns were collected on a Rigaku Ultima IV X-ray diffractometer using Cu K α radiation ($\lambda = 1.5405 \text{ \AA}$) at 35 kV and 25 mA. Inductively coupled plasma (ICP) analysis was carried out on a IRIS Intrepid II XSP spectrometer. Magnetic measurements were performed on a Quantum Design MPMS XLS SQUID magnetometer. The experimental susceptibilities were corrected for the diamagnetism of the constituent atoms (Pascal's tables).

Structure Determination of 1 by Single-Crystal X-ray Analysis. Single-crystal diffraction data of **1**, the Mn(II) compound, were collected at 293 K on a Bruker Apex II CCD area detector equipped with graphite-monochromated Mo K α radiation ($\lambda = 0.71073 \text{ \AA}$). Empirical absorption corrections were applied using the SADABS program.^{24a} The structures were solved by direct methods and refined by full-matrix least-squares methods on F^2 using the SHELXL program, with anisotropic displacement parameters for all non-hydrogen atoms.^{24b} All the hydrogen atoms attached to carbon atoms were placed in calculated positions and refined using the riding model. The water hydrogen atoms attached to O3 were located from the difference Fourier map and refined with restrained O–H and H...H distances (3 restraints using the DFIX instruction). A summary of the crystallographic data and data collection and refinement parameters for compound **1** is provided in Table 1. Crystallographic data in CIF format were deposited with the Cambridge Crystallographic Data Center as CCDC 829471.

Table 1. Crystal Data and Structure Refinement Details for Compound 1

formula	C ₈ H ₈ MnN ₄ O ₅	<i>M_r</i>	295.12
cryst syst	orthorhombic	space group	<i>Pnma</i>
<i>a</i> (Å)	7.6413(7)	<i>b</i> (Å)	7.5660(7)
<i>c</i> (Å)	18.106(2)	<i>V</i> (Å ³)	1046.8(2)
<i>Z</i>	4	ρ_{calcd} (g cm ⁻³)	1.873
μ (mm ⁻¹)	1.283	no. of unique reflns	1226
<i>R</i> _{int}	0.1399	<i>R</i> ₁ (<i>I</i> > 2 σ (<i>I</i>))	0.0683
wR2 (all data)	0.2167		

Structure Determination of 2 by Powder X-ray Analysis. Our efforts to grow crystals of **2** suitable for single-crystal X-ray crystallography were unsuccessful. Since powder X-ray diffraction measurements indicated that the Mn(II) and Fe(II) compounds **1** and **2** are isomorphous, the structure of **2** was determined by powder diffraction using the Reflex and DMol³ programs implemented in the Materials Studio software,^{25a} with the structure of **1** as the starting model. First, the unit cell was refined by the Pawley method^{25b} provided in Reflex. The final Pawley refinement including the pseudo-Voigt peak shape profile parameters, the 20-term background polynomials, the Rietveld asymmetry correction parameters, and the

Bragg–Brentano zero-point shift parameter gave a satisfactory R_{wp} value of 5.85%. The calculated and experimental powder patterns are compared in Figure S1 in the Supporting Information. Second, the atomic coordinates within the fixed unit cell determined by the Pawley refinement were optimized by DFT (density functional theory) lattice energy calculations using the DMol³ module^{25c,d} (BP functional, DND basis set, and effective core potentials for metals, with coarse convergence criteria).

The optimized structure was used as the input for Rietveld refinements^{25e,f} with Reflex. Because of the limited data of powder diffraction, the independent refinements of individual atomic coordinates led to chemically insensible results. Therefore, rigid-body Rietveld refinements were applied, in which the organic ligand, the azide ligand, and the lattice water molecule were defined as independent motion groups, which can translate and rotate with fixed bond distances and angles within each group. A global isotropic temperature factor was applied and refined, because the refinement of independent atomic temperature factors with the limited powder diffraction data is unreliable. The following parameters were also adjusted in the refinements: the pseudo-Voigt peak shape profile parameters, the Bragg–Brentano zero-point shift parameter, the 20-term polynomial background parameters, the Rietveld asymmetry correction parameters, and the March–Dollase parameters for the effects of preferred orientation. The final refinements led to a R_{wp} value of 6.93% with reasonable structure parameters. A summary of the refinement data is given in Table 2. A diagram comparing the calculated and experimental powder patterns and tables giving atomic coordinates and selected bond parameters are supplied in the Supporting Information.

Table 2. Crystal Data and Structure Refinement Details for Compound 2

formula	C ₈ H ₈ FeN ₄ O ₃	M_r	296.02
cryst syst	orthorhombic	space group	<i>Pnma</i>
<i>a</i> (Å)	7.5894(3)	<i>b</i> (Å)	7.3966(3)
<i>c</i> (Å)	18.170(1)	<i>V</i> (Å ³)	1020.0(1)
<i>Z</i>	4	ρ_{calcd} (g cm ⁻³)	1.930
<i>T</i> (K)	293	2θ range (deg)	8.0–50.0
R_{wp}	0.0693	R_p	0.0542

RESULTS AND DISCUSSION

Structural Studies. The structure of the Mn(II) compound **1** was determined by single crystal X-ray analysis, which revealed a chain-based 3D network. As shown in Figure 1, the unique Mn(II) adopts the centrosymmetric *trans*-octahedral [N₂O₄] geometry defined by two azide nitrogen atoms (N1 and N1E) and four carboxylate oxygen atoms (O1, O1A, O2B, and O2C). The Mn–O and Mn–N distances fall in the range 2.132(4)–2.176(4) Å (Table 3). The azide ion and the cmcp

Table 3. Selected Distances (Å) and Angles (deg) for Compound 1^a

Mn1–O2C	2.132(4)	Mn1–O1	2.158(4)
Mn1–N1	2.176(4)		
O2C–Mn1–N1	91.2(2)	O2C–Mn1–O1A	91.47(16)
O1A–Mn1–N1	89.6(2)	O2C–Mn1–O1	88.53(16)
O1–Mn1–N1	90.4(2)	O2B–Mn1–N1	89.5(2)
Mn1D–N1–Mn1	120.7(4)		

^aSymmetry codes: (A) $-x + 1, -y, -z + 1$; (B) $-x + 3/2, -y, z - 1/2$; (C) $x - 1/2, y, -z + 3/2$; (D) $-x + 1, y + 1/2, -z + 1$.

ligand are bisected by the crystallographic mirror plane, which passes through the azide nitrogen atoms and the carboxylate carbon atoms. Adjacent metal ions with $\text{Mn}\cdots\text{Mn} = 3.7830(4)$ Å (*b*/2) are linked by an azide bridge in the μ -1,1 (or end-on, EO) mode and two carboxylate bridges in the *syn*–*syn* mode to yield a formally anionic chain $([\text{Mn}(\mu\text{-N}_3)(\mu\text{-OCO})_2]_n)^{n-}$ along the crystallographic *b* direction. The adjacent octahedrons along the chain share the bridging nitrogen atom with $\text{Mn}\text{-N}\text{-Mn} = 120.7(4)^\circ$ and are slanted toward each other with a dihedral angle of 57.0° between the [MO₄] equatorial planes.

Each $[\text{Mn}(\mu\text{-N}_3)(\mu\text{-OCO})_2]_n^{n-}$ chain is linked to four others by the cationic *N*-methylenepyridinium tethers of the cmcp ligands to produce a neutral 3D MOF. The shortest interchain $\text{M}\cdots\text{M}$ distance is 7.642(1) Å. The interchain space is divided by the bent cmcp ligands into small channels, in which free water molecules are enclosed. Following the approach of topological analysis proposed by O’Keeffe and Yaghi for MOFs with so-called rod secondary building units (SBUs),^{26a,b} the mixed-bridge chain in **1** with the carboxylate C atoms as the points of extension can be regarded as a zigzag ladder SBU, and then the underlying net of **1** is the uninodal 4-connected *sra* net, which has been recognized in some MOFs with dicarboxylate ligands and trivalent metal ions (Al, Cr, Fe) or V^{IV}O, including MIL-47, MIL-53, and MOF-71,²⁶ which are based on neutral chains with $(\mu\text{-X})(\mu\text{-OCO})_2$ bridges (X = OH, O). Note that it is the use of the zwitterionic dicarboxylate ligand which allows us to obtain the neutral networks with divalent metal ions.

The structure of the Fe(II) compound **2**, which is isomorphous with **1**, was determined by powder X-ray analysis with the structure of **1** as the starting model. In going from **1** to **2**, the structural parameters show some differences as a result of the isomorphous substitution of the smaller Fe(II) ion in place of Mn(II). The unit cell contracts by 27 Å³ (~2.6%), and the intrachain Fe \cdots Fe distance (3.6983(2) Å, spanned by the (μ -

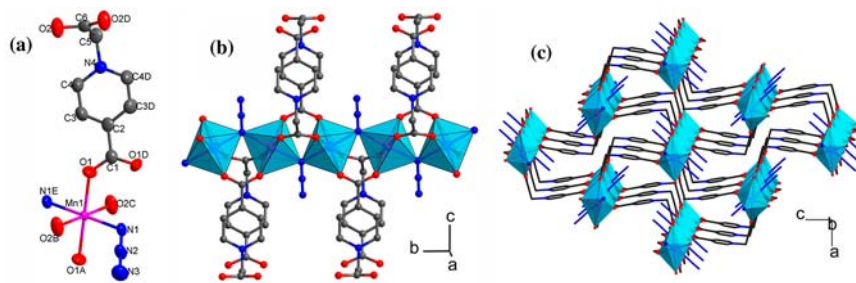


Figure 1. (a) Coordination environments of the unique Mn center in compound **1** (thermal ellipsoids at the 30% probability level). Hydrogen atoms are omitted for clarity. Symmetry codes: (A) $-x + 1, -y, -z + 1$; (B) $-x + 3/2, -y, z - 1/2$; (C) $x - 1/2, y, -z + 3/2$; (D) $-x + 1, y + 1/2, -z + 1$; (E) $1 - x, -1/2 + y, 1 - z$. (b) Chain with mixed carboxylate and azide bridges. (c) 3D network.

$N_3)(\mu\text{-OCO})_2$ bridging motif) in **2** is shorter than Mn...Mn in **1**. The Fe–N/O bond distances (2.111(3)–2.133(3) Å) are also shorter than the Mn counterparts in **1**.

The powder X-ray diffraction (PXRD) patterns of the mixed-metal $Mn_{1-x}Fe_x$ compounds ($0 < x < 1$) are very similar to those of **1** and **2** (see Figure S3 in the Supporting Information), suggesting isomorphism across the whole series for $x = 0-1$. The unit cell parameters of the mixed-metal compounds have been refined from the PXRD data using the CELREF program²⁷ with the orthorhombic cell parameters of **1** as initial values. The results are collected in Table 4. As can be seen, the

Table 4. Unit-Cell Parameters for $Mn_{1-x}Fe_x$ Compounds^a

compd	<i>a</i> (Å)	<i>b</i> (Å)	<i>c</i> (Å)	<i>V</i> (Å ³)
<i>x</i> = 0 (1)	7.6413(7)	7.5660(7)	18.106(2)	1046.8(2)
<i>x</i> = 0.41	7.627(3)	7.549(4)	18.071(7)	1040(1)
<i>x</i> = 0.63	7.622(3)	7.490(4)	18.101(9)	1033(1)
<i>x</i> = 0.76	7.610(3)	7.445(4)	18.130(8)	1027(1)
<i>x</i> = 1 (2)	7.5894(3)	7.3966(3)	18.170(1)	1020.0(1)

^aThe parameters are from single-crystal diffraction for **1** and from powder diffraction for other materials.

cell volume decreases upon the gradual isomorphous displacement of Mn(II) by the smaller Fe(II), and the most appreciable changes are, as expected, along the *b* axis, which is the propagating direction of the chain. The X-ray diffraction results indicate microscopic homogeneity for the mixed-metal materials (for more information, see Figure S3 and its caption in the Supporting Information). The materials can be regarded as solid solutions with a random distribution of Mn(II) and Fe(II) sites.

Magnetic Properties. Compound 1. The magnetic susceptibility of **1** was measured under 1 kOe in the temperature range 2–300 K and is shown as χT and χ versus *T* plots in Figure 2. The measured χT value at 300 K is about

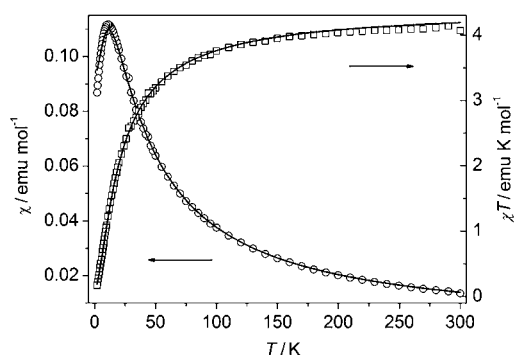


Figure 2. Temperature dependence of χ and χT for **1**. The solid lines represent the fit to a model for the uniform chain (see text).

4.14 emu K mol⁻¹, lower than the spin-only value (4.38 emu mol⁻¹ K) for a high-spin Mn(II) ion. Upon cooling, the χT product decreases monotonically, while χ exhibits a rounded maximum at 11 K. The data above 32 K follow the Curie–Weiss law with $C = 4.38$ emu mol⁻¹ K and $\Theta = -18.1$ K. These features are typical of AF interactions between Mn(II) ions.

Considering the interchain magnetic interactions through the long and methylene-tethered cmpc ligand should be much weaker than the intrachain interactions through the short $(\mu\text{-}N_3)(\mu\text{-OCO})_2$ bridges, the 3D structural framework can be regarded as quasi-1D chains from a magnetic viewpoint. Thus,

the data of **1** over the whole temperature range were fitted to the well-known expression proposed by Fisher for 1D uniform chains of classical spins:²⁸

$$\chi_{\text{chain}} = [Ng^2\beta^2S(S+1)/(3kT)][(1-u)/(1+u)]$$

where $u = \coth[JS(S+1)/kT] - kT/[JS(S+1)]$ and *J* describes the intrachain coupling (spin Hamiltonian $H = -J\sum_i S_i S_{i+1}$ with $S = 5/2$). The best fit led to $J_{\text{MnMn}} = -1.93$ cm⁻¹ and $g = 2.01$. The results confirm 1D antiferromagnetism for **1**.

The $(\mu\text{-}N_3)(\mu\text{-COO})_2$ bridging moiety has been observed in a few Mn(II) compounds reported elsewhere,^{16a-c,29} and it always induces AF coupling. It has been shown that the Mn–N–Mn and Mn–N parameters for the azide bridge are important in determining the magnitude of the coupling: the larger these parameters were, the weaker the coupling.^{16b} The *J* parameters for previous compounds are in the range from -0.9 to -10.1 cm⁻¹, with Mn–N = 2.13–2.23 Å and Mn–N–Mn = 107–118°.^{16a-c} Compound **1** has an intermediate Mn–N distance (2.176(4) Å) but the largest Mn–N–Mn angle (120.7(4)°). The two competing factors compromise to result in a relatively small *J* value (1.93 cm⁻¹).

Compound 2. With an isomorphous structure, **2** is remarkably different from **1** in magnetic behaviors. The χT value of **2** at 300 K is about 4.24 emu mol⁻¹ K. Upon cooling, χ increases monotonically, while the product increases to a sharp maximum at 8.5 K (Figure 3). The Curie–Weiss law is followed above 30

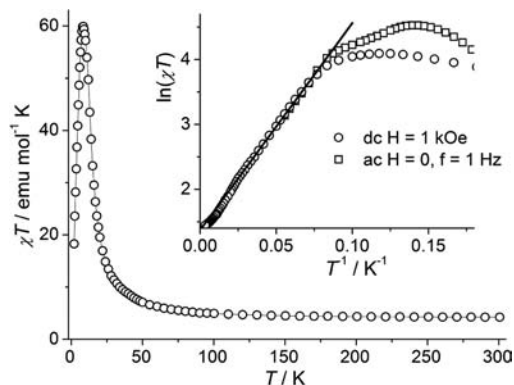


Figure 3. $\chi T(T)$ plot of **2** at 1 kOe. Inset: $\ln(\chi T)$ vs $1/T$ plot for **2**, with the solid line representing the linear fit.

K with $C = 3.90$ emu mol⁻¹ K and $\Theta = 21.5$ K. It is evident that the FO coupling is operative in **2**, in contrast to the AF coupling in **1**. The *C* value is significantly larger than the spin-only value (3.00 emu mol⁻¹ K) for $S = 2$, consistent with the orbitally degenerate $^5T_{2g}$ ground states of Fe^{II} in the octahedral field. The first-order orbital momentum intrinsic to the ground states introduces significant anisotropy into the magnetic properties.

Magnetic exchange between orbitally degenerate metal ions is very complicated, and it is still an open problem that has no exact or general solution.³⁰ In practice, Fe^{II} compounds have been approximately treated by the anisotropic Heisenberg model with isotropic exchange interactions and finite single-ion anisotropy, where the orbital contribution is incorporated into an effective *g* factor and an effective zero-field splitting (ZFS) *D* parameter.^{30b,c} On the basis of the Hamiltonian $H = -J\sum_i S_i S_{i+1} + D\sum_i S_{iz}^2$, and for a uniform chain with uniaxial anisotropy (negative *D* value) and FO coupling (positive *J* value), it has been deduced that the magnetic correlation length increases

exponentially with decreasing temperature, i.e., $\xi \propto \chi T = C \exp(\Delta_\xi/kT)$,² which is also valid for the Ising model. The quantity Δ_ξ corresponds to the energy needed to create a domain wall in the chain and is simply the slope of the $\ln(\chi T)$ versus $1/T$ plot. The scaling analysis has been widely applied in the study of SCMs. Furthermore, for Ising chains or Heisenberg chains with large single-ion anisotropy ($|D/J| > 4/3$), the Δ_ξ energy can be related to the exchange parameter by $\Delta_\xi = 2JS^2$ (note that in some publications the equation is $\Delta_\xi = 4JS^2$, which corresponds to the Hamiltonian with the factor 2 before J). Accordingly, we plotted the $\ln(\chi T) - 1/T$ plot for **2** using dc and ac susceptibility data (Figure 3, inset). It displays a linear region between 11 and 50 K with the slope $\Delta_\xi = 32$ K, confirming the uniaxial anisotropy and the 1D FO character.² Assuming a large anisotropy, which will be confirmed below, the exchange parameter between Fe^{II} ions ($S = 2$) was estimated to be $J_{\text{FeFe}} = 4.0$ K (2.8 cm^{-1}).

The deviation of the $\ln(\chi T) - 1/T$ plot from linearity at lower temperature can be attributed to finite-size effects and weak interchain AF interactions. The finite-size effects occur when the divergence of the correlation length along the chain is suppressed by naturally occurring defects. This effect itself is expected to cause the saturation (but not the decrease) of χT at low temperature, while the occurrence of weak AF interactions between the finite-size chain segments can lead to the decrease.³¹ The decrease can also have a contribution from weak interchain AF interactions in the infinite-chain regime. For the dc measurements at 1 kOe, the field effect is also operative;^{18e} thus, the maximum of χT appears at higher temperature than the maximum of the ac $\chi' T$ data.

The isothermal magnetization of **2** measured at 2 K (Figure 4, top) rises rapidly at low field, confirming the FO interaction. The magnetization increases slowly as the field is increased above 10 kOe, and it does not saturate up to 50 kOe,

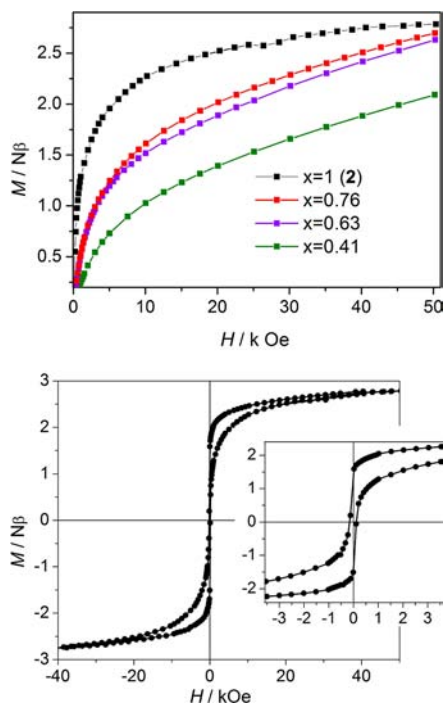


Figure 4. (top) Virgin magnetization curves of **2** and the $\text{Mn}_{1-x}\text{Fe}_x$ compounds at 2 K. (bottom) Hysteresis loop of **2** at 2 K with an enlargement of the low-field region as inset.

suggesting the presence of strong anisotropy. Hysteresis measurements at the same temperature revealed a remnant magnetization of $1.38 \text{ N}\beta$ and a coercive field of 137 Oe (Figure 4, bottom). Furthermore, the field-cooled and zero-field-cooled magnetizations (FCM and ZFCM) measured at 20 Oe (Figure 5) diverge below 6.5 K . The magnetization irreversibility indicates a magnetlike behavior.

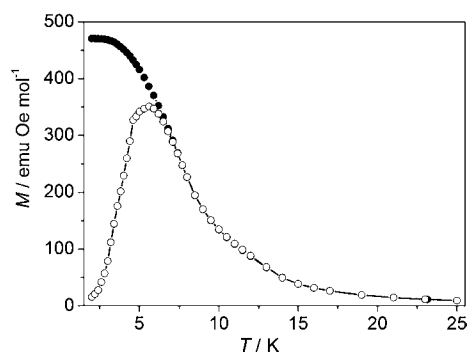


Figure 5. ZFCM (open circles) and FCM (filled circles) plots at 20 Oe for **2**.

ac measurements at zero dc field and different ac frequencies were performed to gain insight into the origin of the magnetlike behavior. As shown in Figure 6, both real (χ') and imaginary

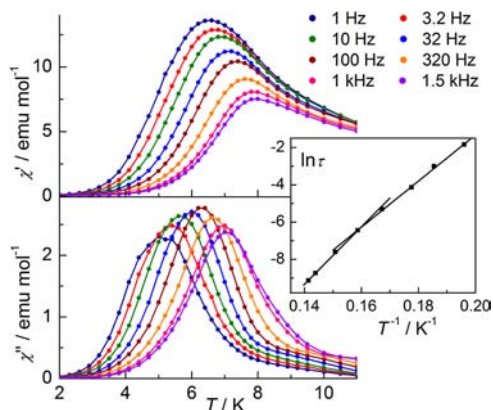


Figure 6. $\chi'(T)$ and $\chi''(T)$ plots for **2** with $H_{\text{dc}} = 0$ and $H_{\text{ac}} = 3 \text{ Oe}$ at 1, 3.3, 10, 33, 100, 330, 1000, and 1500 Hz (from left to right). Inset: solid line representing the least-squares fit of the experimental data to the Arrhenius equation for **2**.

(χ'') susceptibilities are strongly frequency dependent, indicating slow dynamics of magnetization. The peak temperature (T_p) of the $\chi''(T)$ curve shifts from 5.1 to 7.1 K as the frequency is increased from 1 to 1500 Hz . The parameter $\phi = (\Delta T_p/T_p)/\Delta(\log f)$, which is a measure of the frequency dependence,³² was estimated to be 0.11 . This value falls in the typical range ($0.1 \leq \phi \leq 0.3$) for superparamagnets (including SCMs) but is atypical of spin glasses.^{7,32} Plotting $\ln \tau$ against $1/T$ (τ is the relaxation time obtained from the $\chi'' - T$ plots) reveals two thermally activated regimes above and below $T^* = 6.3 \text{ K}$ (Figure 6, inset) following the Arrhenius law with $\Delta_{\tau_1} = 154 \text{ K}$, $\tau_{01} = 3.6 \times 10^{-14} \text{ s}$ and $\Delta_{\tau_2} = 124 \text{ K}$, $\tau_{02} = 4.8 \times 10^{-12} \text{ s}$, respectively. The phenomenon has been observed from some SCMs and can be explained by evoking a crossover from the infinite-chain regime ($T > T^*$) to the finite-size regime ($T < T^*$).² In the infinite regime, $\Delta_{\tau_1} = 2\Delta_\xi + \Delta_A$, where Δ_A

corresponds to the anisotropic barrier for the spin flip inside a domain wall. In the finite-size regime, where the correlation length is limited by defects, $\Delta_{r2} = \Delta_{\xi} + \Delta_A$. Obviously, for such systems, $\Delta_{\xi} = \Delta_{r1} - \Delta_{r2}$. Indeed, for **2**, the difference $\Delta_{r1} - \Delta_{r2} \approx 30$ K is in good agreement with the Δ_{ξ} value (32 K) obtained from the static data. It should be noted that the crossover temperature T^* obtained from the $\ln \tau - 1/T$ plot is lower than the temperature (7 K) at which $\ln(\chi'T)$ reaches a maximum (Figure 3, inset). The discrepancy may be due to the presence of weak interchain AF interactions,^{2a,3d} which can lead to a decrease of $\chi'T$ before the crossover. From the above energy data, it can be estimated that $\Delta_A = \Delta_{r2} - \Delta_{\xi} = 92$ K. The large Δ_A energy suggests strong magnetic anisotropy, and the fact that $\Delta_A \gg \Delta_{\xi}$ indicates a narrow domain wall structure.^{2a} If single-ion anisotropy is assumed within the anisotropic Heisenberg model, it holds that $\Delta_A = |D|S^2$. For **2** ($S = 2$), we have $D_{\text{Fe}} = -23$ K (-16 cm⁻¹). The relatively large D parameter is in the usual range for Fe^{II}.^{30b,33}

Considering that the compound contains 1D FO and anisotropic components separated by CH₂-tethered organic ligands and that the dynamic properties can be explained by the crossover between the infinite- and finite-chain regimes, it is likely that the chain component behaves as a SCM. The attempt time $\tau_{01} = 3.6 \times 10^{-14}$ s is smaller than the values that have been reported for SCMs, which vary in a wide range from 10^{-6} to 10^{-13} s.^{2c} For SCMs showing two relaxation regimes, it is noticeable that the τ_{01} value for the infinite-chain regime is always smaller than τ_{02} for the finite-chain regime, by 2–4 orders of magnitude, as observed for **2**. The τ_0 parameter describes the spin-flip dynamics in the absence of energy barriers and is important in determining the blocking temperature of SCMs, but the influencing factors are still unclear and deserve further studies.

Frequency-dependent ac measurements with **2** at 6.5 K produced a semicircular Cole–Cole diagram (Figure 7), which

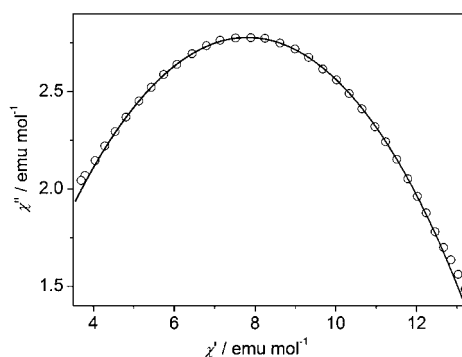


Figure 7. Cole–Cole diagrams for **2** at 6.5 K in the range 0.1–1488 Hz with $H_{\text{dc}} = 0$, $H_{\text{ac}} = 3.0$ Oe. The solid line represents the least-squares fit with a generalized Debye model.

was fitted to the generalized Debye model³⁴ with $\alpha = 0.54$. This value indicates a distribution of relaxation time. The distribution of relaxation time is usual for spin glass dynamics but has also been observed for SCMs and single-molecule magnets (SMMs).^{34b} For SCMs, it may be related to the presence of random defects, which can cause distributions in chain length, magnetic interactions, and anisotropy. The distributions can affect the energy barriers and the relaxation time. We noticed that a wide range (0.01–0.7) of α values have been reported for SCMs.^{2c}

To our knowledge, homospin Fe(II) compounds exhibiting SCM or SCM-like behaviors are still rare. The previously reported examples include (i) a FI-like chain based on the $[\text{Fe}^{\text{II}}_9(\mu\text{-O})_{16}]$ motif ($\mu\text{-O}$ from 2-pyO⁻ or OAc⁻) ($\Delta_{\tau} = 61$ K),^{12a} (ii) a spin-canted AF chain with oxalate bridges ($\Delta_{\tau} = 62$ K),^{12c} (iii) an FO chain with double NCSe bridges ($\Delta_{\tau} = 42$ K),^{12d} and (iv) a 2D MOF based on FO chains with double *syn,anti*- $\mu\text{-COO}$ bridges ($\Delta_{\tau} = 23$ K at $H_{\text{dc}} = 0.1$ T).^{12b} The last example is a metamagnet exhibiting SCM-like dynamics only above the critical field. Our compound **2** is the first 3D Fe(II) MOF behaving as an SCM. It is based on FO chains with a mixed-bridge network and exhibits much larger barriers than previous Fe(II) SCMs. Actually, the barriers of **2** are among the highest values reported thus far for SCMs and are similar to the value (153 K) for $\text{Co}(\text{hfac})_2(\text{NITPhOMe})$, the first SCM.^{1b,2}

As far as the bridging network is concerned, **2** is the first Fe(II) compound with the mixed $(\text{COO})_2(\text{N}_3)$ bridges. Speaking in a wider range, only two Fe(II) compounds with mixed carboxylate and azide bridges have been reported before.³⁵ One is an $[\text{Fe}^{\text{II}}_9]$ cluster with mixed $\mu\text{-carboxylate}$, $\mu_3\text{-alkoxo}$, and $\mu_4\text{-azide}$ bridges, behaving as a SMM,^{35a} the other is a chain compound with mixed $(\mu\text{-formate})(\mu\text{-azide})_2$ bridges, which exhibits intrachain FO interactions and metamagnetic behaviors.^{35b} The FO interaction through the $(\text{COO})(\text{N}_3)_2$ bridges in the formate compound was estimated to be $J = 2.4$ cm⁻¹ by fitting the susceptibility data to the classical-spin model that does not include magnetic anisotropy. For comparison, we have also used the same model to fit the data of **2** and obtained a value of $J = 6.5$ cm⁻¹. Obviously, for the benefit of SCM behaviors, the $(\text{COO})_2(\text{N}_3)$ bridges in **2** induce significantly stronger FO coupling than the $(\text{COO})(\text{N}_3)_2$ bridges in the formate compound. In addition, there are weak hydrogen bonds between neighboring chains in the formate compound. The intrachain and interchain differences between the two compounds may explain why the formate compound behaves as a metamagnet, rather than an SCM.

Thus, we have demonstrated that the isomorphous replacement of Mn(II) by Fe(II) leads to a change from 1D AF behaviors to FO SCM behaviors. The AF-to-FO crossover of the interaction has been observed between Fe(II) and Co(II) for the 1,3-dicyanamide (dca) bridges in the $\text{M}(\text{dca})_2$ series with $\text{M} = \text{Mn}, \text{Fe}, \text{Co}, \text{Ni}$.³⁶ Previous studies have already demonstrated that the $(\mu\text{-COO})_2(\mu\text{-1,1-N}_3)$ bridges induce AF interactions in Mn(II) compounds and FO interactions in Co(II) and Ni(II) compounds.^{16,18a,b} Compound **2** fills the gap between Mn(II) and Co(II) and reveals that the AF-to-FO crossover for the $(\mu\text{-COO})_2(\mu\text{-1,1-N}_3)$ bridges occurs between Mn(II) and Fe(II), as has previously been shown for the $(\mu\text{-COO})(\mu\text{-1,1-N}_3)_2$ bridges.^{17a–d,35b} The crossover has been accounted for by considering the relative change in the competing AF ($t_{2g}\text{-}e_g$) and FO ($t_{2g}\text{-}t_{2g}$ and $e_g\text{-}e_g$) contributions as the number of unpaired t_{2g} electrons in the $t_{2g}^x e_g^y$ configurations decreases.^{17a,36} The observation that the crossovers occur at different points for the dca bridge and the mixed carboxylate–azide bridges implies that the crossover is dependent not only on the relative number of the AF and FO contributions but also on the relative magnitudes of these contributions. Thanks to the crossover from Mn(II) to Fe(II), compound **2** exhibits intrachain FO interactions, which collaborate with the large single-ion anisotropy of Fe(II) to evoke the SCM behaviors.

Mixed-Metal Compounds. The χT – T plots of the $\text{Mn}^{\text{II}}_{1-x}\text{Fe}^{\text{II}}_x$ series are compared in Figure 8. For Mn^{II}-rich

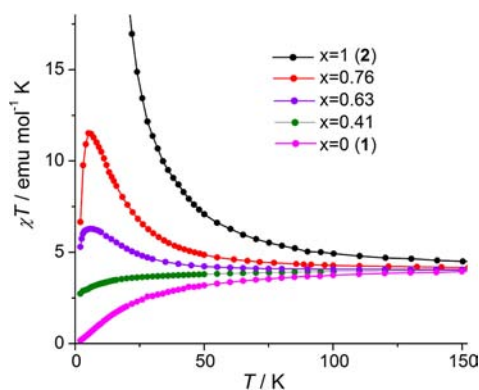


Figure 8. χT - T plots in the low-temperature region for the $\text{Mn}^{1-x}\text{Fe}^x$ compounds.

compounds ($x = 0, 0.41$), χT decreases monotonically with decreasing temperature and the decrease is less rapid for $x = 0.41$. For Fe^{II}-rich species ($x = 0.63, 0.79, 1$), however, χT displays a maximum, which shifts toward higher temperature as x increases. The results of the Curie–Weiss fit are given in Table 5. As the Fe(II) content increases, the Curie constant

Table 5. Select Magnetic Data for the $\text{Mn}^{1-x}\text{Fe}^x$ Compounds

	x				
	0 (1)	0.41	0.63	0.76	1 (2)
$T_{\max}(\chi T)/\text{K}^a$			5.0	5.2	8.5
$C/\text{emu mol}^{-1} \text{K}$	4.38	4.10	3.97	3.95	3.90
Θ/K	-18.1	-3.43	3.64	9.17	21.5
$M_r/N\beta^b$			0.07	0.34	1.59
Δ_r/K			35.5	43.3	154/124
$T_p(\chi'')/\text{K}^c$		<2.0	3.7	4.4	7.0

^aTemperature at which χT shows a maximum at 1 kOe. ^bRemnant magnetization from hysteresis measurements. ^cTemperature at which χ'' at 1 kHz shows a peak.

decreases and the Weiss temperature (Θ) increases from negative (for Mn^{II}-rich compounds) to positive (for Fe^{II}-rich compounds). The comparison clearly indicates a gradual AF-to-FO evolution of the global magnetic behaviors upon Fe(II) substituting Mn(II).

The isothermal magnetization data at 2 K support the AF-to-FO evolution (Figure 4, top): the larger the Fe(II) content, the more rapidly the low-field magnetization increases, and the larger the magnetization at 50 kOe. No appreciable hysteresis was detected for the AF Mn^{II}-rich materials ($x = 0, 0.41$), while the Fe^{II}-rich species exhibit hysteresis loops (Figure 9), with the remnant magnetization decreasing rapidly with the Mn(II) content.

The thermal variation of the ac susceptibilities of the mixed-metal systems at different frequencies are shown in Figure 10. All the materials show nonzero out-of-phase signals below a certain temperature, which shifts to higher temperature as the Fe(II) content increases. Both χ'' and χ' data of the Mn-rich compound with $x = 0.41$ show some degree of frequency dependence but do not show maxima above 2 K. The materials with $x = 0.63, 0.76$ show frequency-dependent maxima in both χ'' and χ' and the maxima shift toward higher temperature as the Fe(II) content increases. The observations indicate that slow relaxation of magnetization occurs and that the blocking

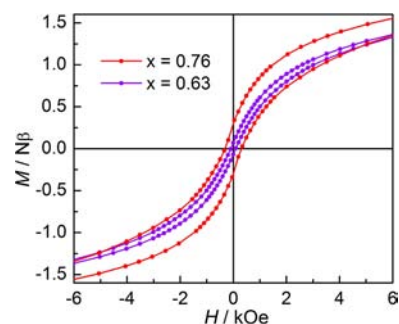


Figure 9. Plots showing the hysteresis for the Fe-rich $\text{Mn}^{1-x}\text{Fe}^x$ compounds.

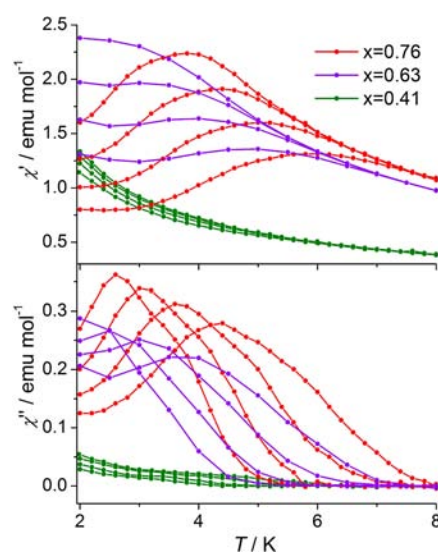


Figure 10. ac susceptibilities of the mixed-metal compounds at frequencies 1, 10, 100, and 1000 Hz (from left to right) with $H_{\text{dc}} = 0$ and $H_{\text{ac}} = 3$ Oe.

temperature increases with the FO and anisotropic component. For $x = 0.63$ and 0.76 , we estimated that $\phi = 0.13$ and 0.18 , respectively, which fall in the usual range for SCMs. The fit to the Arrhenius law gave $\Delta_r = 43.3$ K, $\tau_0 = 8.1 \times 10^{-9}$ s for $x = 0.76$ and $\Delta_r = 35.5$ K, $\tau_0 = 1.1 \times 10^{-8}$ s for $x = 0.63$. These data lie in the range for SCMs, but they should be taken as rough estimates since the χ'' - T peaks are broad and dissymmetric, indicating the presence of additional relaxation processes. This is consistent with the dissymmetric shape of the Cole–Cole diagrams (Figure 11), which cannot be fitted to the generalized Debye model. One possible origin of the additional relaxation is the spin-glass dynamics, which could be associated with the inherent site randomness and the presence of competing AF and FO interactions.^{19,32} The complex dynamics deserve further study.

CONCLUSIONS

The isomorphous Mn(II) and Fe(II) compounds derived from azide and the zwitterionic 1-carboxylatomethylpyridinium-4-carboxylate ligand have been shown to be 3D MOFs in which the formally negative chains with mixed (μ -azide)bis(μ -carboxylate) triple bridges are cross-linked by the positively charged backbones of the zwitterionic ligands. The Mn(II) MOFs display typical 1D AF behaviors. In contrast, with one more d electron per metal center, the Fe(II) counterpart shows

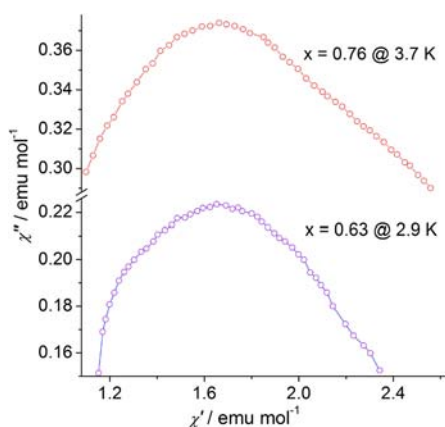


Figure 11. Cole–Cole diagrams for the compounds with $x = 0.76$ (top) and $x = 0.63$ (bottom).

intrachain FO interactions and slow relaxation of magnetization attributable to the anisotropic single-chain components. Taking advantage of the isomorphism between the Mn(II) and Fe(II) MOFs, we have prepared and magnetically studied a series of mixed-metal $\text{Mn}^{II}_{1-x}\text{Fe}^{II}_x$ MOFs with $x = 0.41, 0.63, 0.76$, which intrinsically feature random isotropic/anisotropic sites and competing AF/FO interactions. The materials show a gradual AF-to-FO evolution in overall behaviors as the Fe(II) content increases, and the Fe-rich materials show complex relaxation processes that may arise for mixed SCM and spin-glass mechanisms. A general trend is that the activation energy and the blocking temperature increase with the Fe(II) content, emphasizing the importance of anisotropy for slow relaxation of magnetization. This is the first experimental study of 1D magnetic solid solutions with competing AF/FO interactions and mixed isotropic–anisotropic magnetic sites. It is hoped that this preliminary work may serve to stimulate theoretical and further experimental studies aimed at manipulating SCM and/or spin-glass behaviors in mixed-metal 1D systems.

■ ASSOCIATED CONTENT

📄 Supporting Information

A CIF file giving crystallographic data for compound **1** and tables and figures giving powder diffraction data. This material is available free of charge via the Internet at <http://pubs.acs.org>.

■ AUTHOR INFORMATION

✉ Corresponding Author

*E-mail for E.-Q.G.: eqgao@chem.ecnu.edu.cn.

Notes

The authors declare no competing financial interest.

■ ACKNOWLEDGMENTS

This work was supported by the National Science Foundation of China (NSFC Nos. 91022017 and 21173083) and the Research Fund for the Doctoral Program of Higher Education of China.

■ REFERENCES

(1) (a) Glauber, R. J. *J. Math. Phys.* **1963**, *4*, 294. (b) Caneschi, A.; Gatteschi, D.; Lalioti, N.; Sangregorio, C.; Sessoli, R.; Venturi, G.; Vindigni, A.; Rettori, A.; Pini, M. G.; Novak, M. A. *Angew. Chem., Int. Ed.* **2001**, *40*, 1760. (c) Clérac, R.; Miyasaka, H.; Yamashita, M.; Coulon, C. *J. Am. Chem. Soc.* **2002**, *124*, 12837.

(2) (a) Miyasaka, H.; Clérac, R. *Bull. Chem. Soc. Jpn.* **2005**, *78*, 1725. (b) Coulon, C.; Miyasaka, H.; Clérac, R. *Struct. Bonding (Berlin)* **2006**, *122*, 163. (c) Bogani, L.; Vindigni, A.; Sessoli, R.; Gatteschi, D. *J. Mater. Chem.* **2008**, *18*, 4750. (d) Miyasaka, H.; Julve, M.; Yamashita, M.; Clérac, R. *Inorg. Chem.* **2009**, *48*, 3420. (e) Sun, H.-L.; Wang, Z.-M.; Gao, S. *Coord. Chem. Rev.* **2010**, *254*, 1081. (f) Leong, W. L.; Vittal, J. J. *Chem. Rev.* **2011**, *111*, 688.

(3) (a) Balanda, M.; Rams, M.; Nayak, S. K.; Tomkowicz, Z.; Haase, W.; Tomala, K.; Yakhmi, J. V. *Phys. Rev. B* **2006**, *74*, 224421. (b) Bernot, K.; Bogani, L.; Caneschi, A.; Gatteschi, D.; Sessoli, R. *J. Am. Chem. Soc.* **2006**, *128*, 7947. (c) Ishii, N.; Ishida, T.; Nogami, T. *Inorg. Chem.* **2006**, *45*, 3837. (d) Miyasaka, H.; Madanbashi, T.; Sugimoto, K.; Nakazawa, Y.; Wernsdorfer, W.; Sugiura, K.-I.; Yamashita, M.; Coulon, C.; Clérac, R. *Chem. Eur. J.* **2006**, *12*, 7028. (e) Ishii, N.; Okamura, Y.; Chiba, S.; Nogami, T.; Ishida, T. *J. Am. Chem. Soc.* **2008**, *130*, 24. (f) Sessoli, R. *Angew. Chem., Int. Ed.* **2008**, *47*, 5508. (g) Bernot, K.; Luzon, J.; Caneschi, A.; Gatteschi, D.; Sessoli, R.; Bogani, L.; Vindigni, A.; Rettori, A.; Pini, M. G. *Phys. Rev. B* **2009**, *79*, 134419. (h) Liu, R. N.; Li, L. C.; Wang, X. L.; Yang, P. P.; Wang, C.; Liao, D. Z.; Sutter, J. P. *Chem. Commun.* **2010**, *46*, 2566.

(4) (a) Lecren, L.; Wernsdorfer, W.; Li, Y. G.; Vindigni, A.; Miyasaka, H.; Clérac, R. *J. Am. Chem. Soc.* **2007**, *129*, 5045. (b) Saitoh, A.; Miyasaka, H.; Yamashita, M.; Clérac, R. *J. Mater. Chem.* **2007**, *17*, 2002. (c) Miyasaka, H.; Saitoh, A.; Yamashita, M.; Clérac, R. *Dalton Trans.* **2008**, 2422. (d) Coulon, C.; Clérac, R.; Wernsdorfer, W.; Colin, T.; Miyasaka, H. *Phys. Rev. Lett.* **2009**, *102*, 167204. (e) Miyasaka, H.; Takayama, K.; Saitoh, A.; Furukawa, S.; Yamashita, M.; Clérac, R. *Chem. Eur. J.* **2010**, *16*, 3656.

(5) (a) Liu, T.; Zhang, Y. J.; Kanegawa, S.; Sato, O. *J. Am. Chem. Soc.* **2010**, *132*, 8250. (b) Dong, D. P.; Zheng, H.; Zhao, L.; Zhuang, P. F.; Liu, T.; He, C.; Duan, C. Y. *Sci. China Chem.* **2012**, *55*, 1018. (c) Miyasaka, H.; Madanbashi, T.; Saitoh, A.; Motokawa, N.; Ishikawa, R.; Yamashita, M.; Bahr, S.; Wernsdorfer, W.; Clérac, R. *Chem. Eur. J.* **2012**, *18*, 3942. (d) Senapati, T.; Pichon, C.; Ababei, R.; Mathonière, C.; Clérac, R. *Inorg. Chem.* **2012**, *51*, 3796. (e) Wang, S.; Ding, X. H.; Li, Y. H.; Huang, W. *Coord. Chem. Rev.* **2012**, *256*, 439. (f) Visinescu, D.; Madalan, A. M.; Andruh, M.; Duhayon, C.; Sutter, J. P.; Ungur, L.; Van den Heuvel, W.; Chibotaru, L. F. *Chem. Eur. J.* **2009**, *15*, 11808. (6) (a) Guo, J. F.; Wang, X. T.; Wang, B. W.; Xu, G. C.; Gao, S.; Szeto, L.; Wong, W. T.; Wong, W. Y.; Lau, T. C. *Chem. Eur. J.* **2010**, *16*, 3524. (b) Harris, T. D.; Bennett, M. V.; Clérac, R.; Long, J. R. *J. Am. Chem. Soc.* **2010**, *132*, 3980. (c) Feng, X. W.; Harris, T. D.; Long, J. R. *Chem. Sci.* **2011**, *2*, 1688. (d) Harris, T. D.; Coulon, C.; Clérac, R.; Long, J. R. *J. Am. Chem. Soc.* **2011**, *133*, 123. (e) Yoon, J. H.; Ryu, D. W.; Choi, S. Y.; Kim, H. C.; Koh, E. K.; Tao, J.; Hong, C. S. *Chem. Commun.* **2011**, *47*, 10416. (f) Feng, X. W.; Liu, J. J.; Harris, T. D.; Hill, S.; Long, J. R. *J. Am. Chem. Soc.* **2012**, *134*, 7521. (g) Lee, J.; Lim, K.; Yoon, J.; Ryu, D.; Koo, B.; Koh, E.; Hong, C. *Sci. China Chem.* **2012**, *55*, 1012.

(7) (a) Pardo, E.; Train, C.; Lescouezec, R.; Journaux, Y.; Pasan, J.; Ruiz-Perez, C.; Delgado, F. S.; Ruiz-Garcia, R.; Lloret, F.; Paulsen, C. *Chem. Commun.* **2010**, *46*, 2322. (b) Ferrando-Soria, J.; Cangussu, D.; Eslava, M.; Journaux, Y.; Lescouezec, R.; Julve, M.; Lloret, F.; Pasan, J.; Ruiz-Perez, C.; Lhotel, E.; Paulsen, C.; Pardo, E. *Chem. Eur. J.* **2011**, *17*, 12482. (c) Ferrando-Soria, J.; Pardo, E.; Ruiz-Garcia, R.; Cano, J.; Lloret, F.; Julve, M.; Journaux, Y.; Pasan, J.; Ruiz-Perez, C. *Chem. Eur. J.* **2011**, *17*, 2176. (d) Coronado, E.; Galán-Mascarós, J. R.; Martí-Gastaldo, C. *CrystEngComm* **2009**, *11*, 2143. (e) Cariati, E.; Ugo, R.; Santoro, G.; Tordin, E.; Sorace, L.; Caneschi, A.; Sironi, A.; Macchi, P.; Casati, N. *Inorg. Chem.* **2010**, *49*, 10894. (f) Coronado, E.; Galán-Mascarós, J. R.; Martí-Gastaldo, C. *J. Am. Chem. Soc.* **2008**, *130*, 14987.

(8) (a) Kajiwara, T.; Nakano, M.; Kaneko, Y.; Takaishi, S.; Ito, T.; Yamashita, M.; Igashira-Kamiyama, A.; Nojiri, H.; Ono, Y.; Kojima, N. *J. Am. Chem. Soc.* **2005**, *127*, 10150. (b) Tanaka, H.; Kajiwara, T.; Kaneko, Y.; Takaishi, S.; Yamashita, M. *Polyhedron* **2007**, *26*, 2105. (c) Kajiwara, T.; Tanaka, H.; Yamashita, M. *Pure Appl. Chem.* **2008**, *80*, 2297. (d) Kajiwara, T.; Tanaka, H.; Nakano, M.; Takaishi, S.; Nakazawa, Y.; Yamashita, M. *Inorg. Chem.* **2010**, *49*, 8358. (e) Zheng, Y.-Z.; Xue, W.; Zhang, W.-X.; Tong, M.-L.; Chen, X.-M.; Grandjean,

F.; Long, G. J.; Ng, S.-W.; Panissod, P.; Drillon, M. *Inorg. Chem.* **2009**, *48*, 2028.

(9) (a) Liu, T. F.; Fu, D.; Gao, S.; Zhang, Y. Z.; Sun, H. L.; Su, G.; Liu, Y. J. *J. Am. Chem. Soc.* **2003**, *125*, 13976. (b) Hu, B.-W.; Zhao, J.-P.; Yang, Q.; Zhang, X.-F.; Evangelisti, M.; Sanudo, E. C.; Bu, X.-H. *Dalton Trans.* **2010**, *39*, 11210. (c) Li, Z. X.; Zeng, Y. F.; Ma, H.; Bu, X. H. *Chem. Commun.* **2010**, *46*, 8540. (d) Song, X. Y.; Yang, P. P.; Mei, X. L.; Li, L. C.; Liao, D. Z. *Eur. J. Inorg. Chem.* **2010**, 1689. (e) Zhao, J.-P.; Hu, B.-W.; Zhang, X.-F.; Yang, Q.; El, F. M. S.; Ribas, J.; Bu, X.-H. *Inorg. Chem.* **2010**, *49*, 11325. (f) Yoon, J. H.; Lee, J. W.; Ryu, D. W.; Yoon, S. W.; Suh, B. J.; Kim, H. C.; Hong, C. S. *Chem. Eur. J.* **2011**, *17*, 3028.

(10) (a) Zheng, Y.-Z.; Tong, M.-L.; Zhang, W.-X.; Chen, X.-M. *Angew. Chem., Int. Ed.* **2006**, *45*, 6310. (b) Zheng, Y. Z.; Xue, W.; Tong, M. L.; Chen, X. M.; Zheng, S. L. *Inorg. Chem.* **2008**, *47*, 11202. (c) Liu, C. M.; Zhang, D. Q.; Zhu, D. B. *Inorg. Chem.* **2009**, *48*, 4980. (d) Zhang, S. Y.; Shi, W.; Lan, Y. H.; Xu, N.; Zhao, X. Q.; Powell, A. K.; Zhao, B.; Cheng, P.; Liao, D. Z.; Yan, S. P. *Chem. Commun.* **2011**, *47*, 2859. (e) Zhang, W. X.; Shiga, T.; Miyasaka, H.; Yamashita, M. *J. Am. Chem. Soc.* **2012**, *134*, 6908. (f) Zhao, J. P.; Yang, Q.; Liu, Z. Y.; Zhao, R.; Hu, B. W.; Du, M.; Chang, Z.; Bu, X. H. *Chem. Commun.* **2012**, *48*, 6568.

(11) (a) Sun, Z. M.; Prosvirin, A. V.; Zhao, H. H.; Mao, J. G.; Dunbar, K. R. *J. Appl. Phys.* **2005**, *97*, 10B305. (b) Pali, A. V.; Ostrovsky, S. M.; Klokishner, S. I.; Reu, O. S.; Sun, Z. M.; Prosvirin, A. V.; Zhao, H. H.; Mao, J. G.; Dunbar, K. R. *J. Phys. Chem. A* **2006**, *110*, 14003. (c) Pali, A. V.; Reu, O. S.; Ostrovsky, S. M.; Klokishner, S. I.; Tsukerblat, B. S.; Sun, Z. M.; Mao, J. G.; Prosvirin, A. V.; Zhao, H. H.; Dunbar, K. R. *J. Am. Chem. Soc.* **2008**, *130*, 14729.

(12) (a) Przybylak, S. W.; Tuna, F.; Teat, S. J.; Wimpenny, R. E. P. *Chem. Commun.* **2008**, 1983. (b) Zheng, Y.-Z.; Xue, W.; Tong, M.-L.; Chen, X.-M.; Grandjean, F.; Long, G. J. *Inorg. Chem.* **2008**, *47*, 4077. (c) Keene, T. D.; Zimmermann, I.; Neels, A.; Sereda, O.; Hauser, J.; Bonin, M.; Hursthouse, M. B.; Price, D. J.; Decurtins, S. *Dalton Trans.* **2010**, *39*, 4937. (d) Boeckmann, J.; Wriedt, M.; Näther, C. *Chem. Eur. J.* **2012**, *18*, 5284.

(13) (a) Huang, Y. G.; Wang, X. T.; Jiang, F. L.; Gao, S.; Wu, M. Y.; Gao, Q.; Wei, W.; Hong, M. C. *Chem. Eur. J.* **2008**, *14*, 10340. (b) Zheng, Y.-Z.; Lan, Y.; Wernsdorfer, W.; Anson, C. E.; Powell, A. K. *Chem. Eur. J.* **2009**, *15*, 12566. (c) Luo, F.; Liao, Z.-W.; Song, Y.-M.; Huang, H.-X.; Tian, X.-Z.; Sun, G.-M.; Zhu, Y.; Yuan, Z.-Z.; Luo, M.-B.; Liu, S.-J.; Xu, W.-Y.; Feng, X.-F. *Dalton Trans.* **2011**, *40*, 12651.

(14) (a) Zhang, X.-M.; Hao, Z.-M.; Zhang, W.-X.; Chen, X.-M. *Angew. Chem., Int. Ed.* **2007**, *46*, 3456. (b) Ouellette, W.; Prosvirin, A. V.; Whitenack, K.; Dunbar, K. R.; Zubieta, J. *Angew. Chem., Int. Ed.* **2009**, *48*, 2140. (c) Ding, M.; Wang, B. W.; Wang, Z. M.; Zhang, J. L.; Fuhr, O.; Fenske, D.; Gao, S. *Chem. Eur. J.* **2012**, *18*, 915.

(15) (a) Batten, S. R.; Champness, N. R.; Chen, X. M.; Garcia-Martinez, J.; Kitagawa, S.; Öhrström, L.; O'Keeffe, M.; Suh, M. P.; Reedijk, J. *CrystEngComm* **2012**, *14*, 3001. (b) Kurmoo, M. *Chem. Soc. Rev.* **2009**, *38*, 1353.

(16) (a) Tian, C. Y.; Sun, W. W.; Jia, Q. X.; Tian, H.; Gao, E. Q. *Dalton Trans.* **2009**, 6109. (b) Wang, Y. Q.; Jia, Q. X.; Wang, K.; Cheng, A. L.; Gao, E. Q. *Inorg. Chem.* **2010**, *49*, 1551. (c) Wang, Y. Q.; Sun, Q.; Yue, Q.; Cheng, A. L.; Song, Y.; Gao, E. Q. *Dalton Trans.* **2011**, *40*, 10966. (d) Sun, W. W.; Tian, C. Y.; Jing, X. H.; Wang, Y. Q.; Gao, E. Q. *Chem. Commun.* **2009**, 4741. (e) Ma, Y.; Li, X. B.; Yi, X. C.; Jia, Q. X.; Gao, E. Q.; Liu, C. M. *Inorg. Chem.* **2010**, *49*, 8092. (f) Wang, Y. Q.; Wang, K.; Sun, Q.; Tian, H.; Gao, E. Q.; Song, Y. *Dalton Trans.* **2009**, 9854.

(17) (a) Ma, Y.; Zhang, J. Y.; Cheng, A. L.; Sun, Q.; Gao, E. Q.; Liu, C. M. *Inorg. Chem.* **2009**, *48*, 6142. (b) Ma, Y.; Wen, Y. Q.; Zhang, J. Y.; Gao, E. Q.; Liu, C. M. *Dalton Trans.* **2010**, *39*, 1846. (c) Ma, Y.; Wang, K.; Gao, E. Q.; Song, Y. *Dalton Trans.* **2010**, *39*, 7714. (d) Wen, Y. Q.; Ma, Y.; Wang, Y. Q.; Zhang, X. M.; Gao, E. Q. *Inorg. Chem. Commun.* **2012**, *20*, 46. (e) Ma, Y.; Bandeira, N. A. G.; Robert, V.; Gao, E. Q. *Chem. Eur. J.* **2011**, *17*, 1988.

(18) (a) Zhang, X. M.; Wang, Y. Q.; Wang, K.; Gao, E. Q.; Liu, C. M. *Chem. Commun.* **2011**, *47*, 1815. (b) Wang, Y. Q.; Sun, W. W.; Wang,

Z. D.; Jia, Q. X.; Gao, E. Q.; Song, Y. *Chem. Commun.* **2011**, *47*, 6386. (c) Jia, Q. X.; Tian, H.; Zhang, J. Y.; Gao, E. Q. *Chem. Eur. J.* **2011**, *17*, 1040. (d) Li, X. B.; Zhang, J. Y.; Wang, Y. Q.; Song, Y.; Gao, E. Q. *Chem. Eur. J.* **2011**, *17*, 13883. (e) Wang, Y. Q.; Zhang, X. M.; Li, X. B.; Wang, B. W.; Gao, E. Q. *Inorg. Chem.* **2011**, *50*, 6314. (f) Zhang, X. M.; Wang, K.; Wang, Y. Q.; Gao, E. Q. *Dalton Trans.* **2011**, *40*, 12742.

(19) (a) DeFotis, G. C.; Pohl, C.; Pugh, S. A.; Sinn, E. J. *Chem. Phys.* **1984**, *80*, 2079. (b) DeFotis, G. C.; Coker, G. S.; Jones, J. W.; Branch, C. S.; King, H. A.; Bergman, J. S.; Lee, S.; Goodey, J. R. *Phys. Rev. B* **1998**, *58*, 12178. (c) Restrepo, J.; Greneche, J. M. *Phys. Rev. B* **2005**, *71*, 064406.

(20) (a) Katsumata, K.; Shapiro, S. M.; Matsuda, M.; Shirane, G.; Tschendler, J. *Phys. Rev. B* **1992**, *46*, 14906. (b) DeFotis, G. C.; Wallo, C. D.; Smith, R. L.; Bodkin, D. B.; Mirabilio, G. L.; Leftwich, T. R.; Kim, M. G.; Reed, Z. D. *Phys. Rev. B* **2005**, *71*, 224415 and references therein. (c) Pirogov, A. N.; Park, J. G.; Ermolenko, A. S.; Korolev, A. V.; Kuchin, A. G.; Lee, S.; Choi, Y. N.; Park, J.; Ranot, M.; Yi, J.; Gerasimov, E. G.; Dorofeev, Y. A.; Vokhmyanin, A. P.; Podlesnyak, A. A.; Swainson, I. P. *Phys. Rev. B* **2009**, *79*, 174412 and references therein.

(21) (a) Vaz, M. G. F.; Pinheiro, L. M. M.; Stumpf, H. O.; Alcântara, A. F. C.; Golhen, S.; Ouahab, L.; Cador, O.; Mathonière, C.; Kahn, O. *Chem. Eur. J.* **1999**, *5*, 1486. (b) Lappas, A.; Wills, A. S.; Green, M. A.; Prassides, K.; Kurmoo, M. *Phys. Rev. B* **2003**, *67*, 144406. (c) Pajeroski, D. M.; Gardner, J. E.; Talham, D. R.; Meisel, M. W. *J. Am. Chem. Soc.* **2009**, *131*, 12927. (d) Yusuf, S. M.; Thakur, N.; Kumar, A.; Yakhmi, J. V. *J. Appl. Phys.* **2010**, *107*, 053902. (e) Idobata, Y.; Zhou, B.; Kobayashi, A.; Kobayashi, H. *J. Am. Chem. Soc.* **2012**, *134*, 871.

(22) (a) Beghidja, A.; Rogez, G.; Rabu, P.; Welter, R.; Drillon, M. *J. Mater. Chem.* **2006**, *16*, 2715. (b) Zeng, M.-H.; Wang, B.; Wang, X.-Y.; Zhang, W.-X.; Chen, X.-M.; Gao, S. *Inorg. Chem.* **2006**, *45*, 7069. (c) Rodríguez-Díezguéz, A.; Palacios, M. A.; Sironi, A.; Colacio, E. *Dalton Trans.* **2008**, 2887. (d) Zhao, J. P.; Hu, B. W.; Zhang, X. F.; Yang, Q. A.; El Fallah, M. S.; Ribas, J.; Bu, X. H. *Inorg. Chem.* **2010**, *49*, 11325. (e) Huang, L. F.; Ji, C. C.; Lu, Z. Z.; Yao, X. Q.; Hu, J. S.; Zheng, H. G. *Dalton Trans.* **2011**, *40*, 3183. (f) Coronado, E.; Galán-Mascarós, J. R.; Gómez-García, C. J.; Martínez-Agudo, J. M. *Synth. Met.* **2001**, *122*, 501. (g) Coronado, E.; Galán-Mascarós, J. R.; Gómez-García, C. J.; Martínez-Agudo, J. M. *Adv. Mater.* **1999**, *11*, 558.

(23) Wang, X.-B.; Dacres, J. E.; Yang, X.; Broadus, K. M.; Lis, L.; Wang, L.-S.; Kass, S. R. *J. Am. Chem. Soc.* **2003**, *125*, 296.

(24) (a) Sheldrick, G. M. *SADABS, Program for Empirical Absorption Correction*; University of Göttingen, Göttingen, Germany, 1996. (b) Sheldrick, G. M. *SHELXTL*; Bruker Analytical X-ray Instruments Inc., Madison, WI, 1998.

(25) (a) *Materials Studio 6.1*; Accelrys Software Inc., San Diego, CA, 2009. (b) Pawley, G. S. *J. Appl. Crystallogr.* **1981**, *14*, 357. (c) Delley, B. J. *Chem. Phys.* **1990**, *92*, 508. (d) Delley, B. J. *Chem. Phys.* **2000**, *113*, 7756. (e) Rietveld, H. M. *J. Appl. Crystallogr.* **1969**, *2*, 65. (f) Young, R. A. *The Rietveld Method*; Oxford University Press: Oxford, U.K., 1993; IUCr Monographs of Crystallography 5.

(26) (a) Rosi, N. L.; Kim, J.; Eddaoudi, M.; Chen, B. L.; O'Keeffe, M.; Yaghi, O. M. *J. Am. Chem. Soc.* **2005**, *127*, 1504. (b) O'Keeffe, M.; Yaghi, O. M. *Chem. Rev.* **2012**, *112*, 675. (c) Barthelet, K.; Marrot, J.; Riou, D.; Feréy, G. *Angew. Chem., Int. Ed.* **2001**, *41*, 281. (d) Serre, C.; Millange, F.; Thouvenot, C.; Nogues, M.; Marsolier, G.; Louer, D.; Feréy, G. *J. Am. Chem. Soc.* **2002**, *124*, 13519.

(27) Laugier, J.; Bochu, B. *LMGP, Suite of Programs for the Interpretation of X-ray Experiments*; ENSP/Laboratoire des Matériaux et de Génie Physique: Saint Martin d'Hères, France; <http://www.inpg.fr/LMGP>.

(28) Fisher, M. E. *Am. J. Phys.* **1964**, *32*, 343.

(29) (a) Wang, L.; Liu, Z.; Zhang, C.; Liu, Z.; Liao, D.; Jiang, Z.; Yan, S. *Sci. China, Ser. B: Chem.* **2003**, *46*, 533. (b) Cheng, L.; Zhang, W. X.; Ye, B. H.; Lin, J. B.; Chen, X. M. *Eur. J. Inorg. Chem.* **2007**, 2668.

(30) (a) Borrás-Almenar, J. J.; Clemente-Juan, J. M.; Coronado, E.; Pali, A. V.; Tsukerblat, B. S. *J. Phys. Chem. A* **1998**, *102*, 200. (b) Konar, S.; Zangrando, E.; Drew, M. G. B.; Mallah, T.; Ribas, J.

Chaudhuri, N. R. *Inorg. Chem.* **2003**, *42*, 5966. (c) Venkatakrishnan, T. S.; Sahoo, S.; Brefuel, N.; Duhayon, C.; Paulsen, C.; Barra, A. L.; Ramasesha, S.; Sutter, J. P. *J. Am. Chem. Soc.* **2010**, *132*, 6047.

(31) (a) Bogani, L.; Sessoli, R.; Pini, M. G.; Rettori, A.; Novak, M. A.; Rosa, P.; Massi, M.; Fedi, M. E.; Giuntini, L.; Caneschi, A.; Gatteschi, D. *Phys. Rev. B* **2005**, *72*, 064406. (b) Bogani, L.; Caneschi, A.; Fedi, M.; Gatteschi, D.; Massi, M.; Novak, M. A.; Pini, M. G.; Rettori, A.; Sessoli, R.; Vindigni, A. *Phys. Rev. Lett.* **2004**, *92*, 207204.

(32) Mydosh, J. A. *Spin Glasses: An Experimental Introduction*; Taylor & Francis: London, 1993.

(33) (a) Carlin, R. L. *Magnetochemistry*; Springer-Verlag: Berlin, Heidelberg, 1986. (b) Kahn, O. *Molecular Magnetism*; VCH: New York, 1993. (c) Boca, R. *Coord. Chem. Rev.* **2004**, *248*, 757.

(34) (a) Cole, K. S.; Cole, R. H. *J. Chem. Phys.* **1941**, *9*, 341. (b) Aubin, S. M. J.; Sun, Z.; Pardi, L.; Krzystek, J.; Folting, K.; Brunel, L.-C.; Rheingold, A. L.; Christou, G.; Hendrickson, D. N. *Inorg. Chem.* **1999**, *38*, 5329.

(35) (a) Boudalis, A. K.; Sanakis, Y.; Clemente-Juan, J. M.; Donnadieu, B.; Nastopoulos, V.; Mari, A.; Coppel, Y.; Tuchagues, J. P.; Perlepes, S. P. *Chem. Eur. J.* **2008**, *14*, 2514. (b) Liu, T.; Zhang, Y. J.; Wang, Z. M.; Gao, S. *Inorg. Chem.* **2006**, *45*, 2782.

(36) (a) Batten, S. R.; Murray, K. S. *Coord. Chem. Rev.* **2003**, *246*, 103. (b) Batten, S. R.; Jensen, P.; Kepert, C. J.; Kurmoo, M.; Moubarak, B.; Murray, K. S.; Price, D. J. *J. Chem. Soc., Dalton Trans.* **1999**, 2987. (c) Kmety, C. R.; Huang, Q.; Lynn, J. W.; Erwin, R. W.; Manson, J. L.; McCall, S.; Crow, J. E.; Stevenson, K. L.; Miller, J. S.; Epstein, A. J. *Phys. Rev. B* **2000**, *62*, 5576.